End-Fire Substrate Integrated Waveguide Beam-Forming System for 5G Applications

Chad Bartlett, Sara Salem Hesari, Jens Bornemann
Department of Electrical and Computer Engineering, University of Victoria, Victoria, Canada
cbartlet@uvic.ca

***Abstract*—This paper presents the simulated and measured results of a substrate integrated beam-forming network that combines the steering capabilities of a 4x4 Butler matrix and the horizontal polarization of a corrugated Vivaldi antenna array for 5G end-fire applications. The system demonstrates a ±25º sweep of the main beams as well as a gain that ranges between 8.7 dB and 11.7 dB at a center frequency of 25 GHz. Good agreement between experimental and simulated results validates the design approach.**

Keywords—Substrate Integrated Waveguide (SIW), Vivaldi antenna, Butler matrix, end-fire, polarization

I. INTRODUCTION

Due to the ever-increasing demand for wider bandwidth, progressive research into millimetre-wave hardware for cellular and backhaul applications has become vital for the standardization and commercialization of 5G networks. Substrate integrated waveguide (SIW) technology is a compelling candidate for overcoming many of the challenges faced when designing cost-effective, high-gain, low-loss systems in millimetre-wave technologies [1]. Advancements in this field by [2-7] and many others have demonstrated notable results with respect to SIW slot antenna beam-forming networks. These contributions have demonstrated the attributes of broadside antenna arrays.

This paper incorporates the basis of these designs with additional components such as phase shifters and corrugated antennas in order to achieve a horizontally polarized beam-forming network for end-fire applications.

II. ANTENNA FEED-NETWOK

The beam-forming network is in the arrangement of a 4x4 Butler matrix [8]. Fig. 1 depicts the ideal Butler matrix, which is comprised of four hybrid couplers, four phase-shifters, and two cross-over couplers. Detailed design techniques for each component can be reviewed in literature [2-5]. For this system, the phase shifters φ_1 and φ_2 were chosen to be 135° and 0°, respectively, with reference to the cross-over couplers. The input ports are labeled 1 through 4, and the outputs that feed the antenna array are labeled 5 through 8. By exciting one of the input ports, the Butler matrix divides the power to each of the four outputs while simultaneously isolating the un-used input ports. By design, the phase difference between each of the output ports will be determined by the respective input port selected for excitation. For input ports 1 through 4, the respective phase differences at the outputs become +135°, -45°, +45°, -135° due to the specifics of each signal's path.

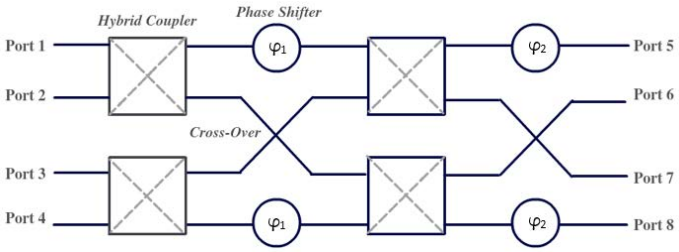

Fig. 1. Ideal Butler matrix.

Each of the aforementioned components used to design the Butler matrix, as well as the output antenna array, are fabricated on a Rogers RT/duroid 6002 substrate, with a thickness of 0.508 mm, and a dielectric constant of 2.94. Simulations are conducted in Mician's μWaveWizard software using mode matching techniques as well as in CST's full-wave frequency simulator. The metalized via spacing for the SIW walls a_{SIW} is calculated to be 5.288mm using (1) from [9], where the diameter d of the vias is set to be 0.3 mm, the spacing p is 0.56 mm, and the effective waveguide width W_{equi} is found from (2).

$$a_{SIW} = W_{equi} + p\left(0.766e^{0.4482d/p} - 1.176e^{-1.214d/p}\right) \quad (1)$$

$$W_{equi} = \frac{c}{2f_c\sqrt{\varepsilon_r}} \quad (2)$$

The results of the Butler matrix are compared in both μWaveWizard and CST. Fig. 2 and Fig. 3 depict the lossless scattering parameters over a frequency range of 23 GHz to 27 GHz that are associated with the excitation of input port 1 and port 2, respectively. The return losses and isolation are better than 20 dB over a range of 23.5 GHz to 26.3 GHz for port 1, and better than 20 dB over a range of 23.8 GHz to 26.7 GHz for port 2. Upon exciting ports 1 and 2, coupling levels fall within the range of 6.1 dB with ±1.3 dB dispersion and 6.1 dB with ±2.1 dB dispersion, respectively. The bandwidth of the full Butler matrix is found to be approximately 10.1 %.

Fig. 4 depicts the simulated phase differences between adjacent output ports while exciting each of the input ports independently.

This work was supported by the National Sciences and Engineering Research Council (NSERC) of Canada.

978-1-5386-1338-2/18/$31.00 ©2018

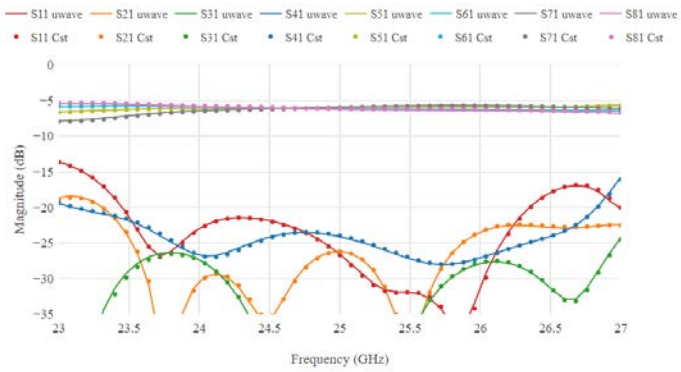

Fig. 2. *S*x1 parameters of Butler matrix.

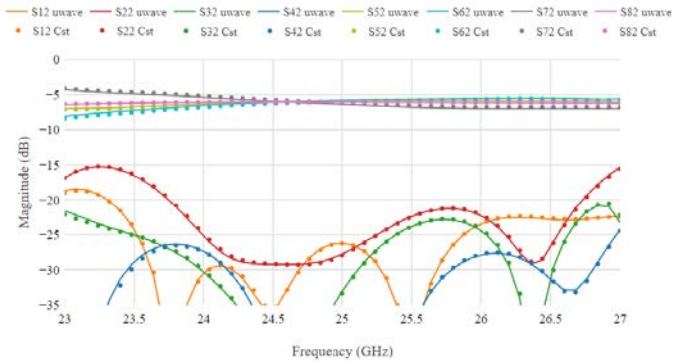

Fig. 3. *S*x2 parameters of Butler matrix.

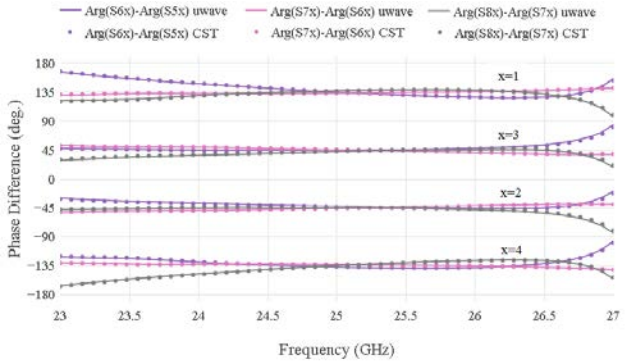

Fig. 4. Simulated phase difference at output ports.

At 25 GHz, port 1 and port 4 have a phase error of approximately 4.8°, while port 2 and port 3 have a phase error of approximately 5.0°. Over the full frequency range investigated, the upper and lower bounds start to deviate where ports 1 and 4 have a maximum phase error of 53.5°, and ports 2 and 3 have a maximum phase error of 66.5°.

III. Antenna Array

For the antenna array, corrugated antipodal Vivaldi antennas are selected for their ability to suppress the vertical polarization component of the beam while still being able to easily pass the horizontal component. The general design is

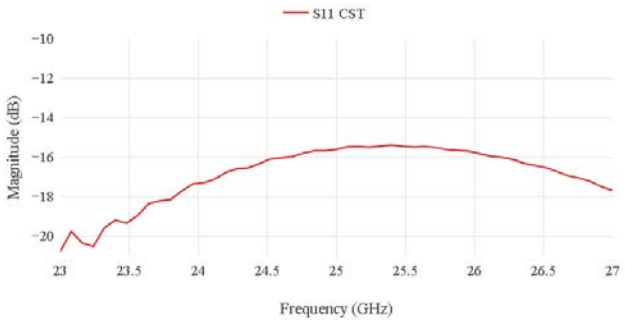

Fig. 6. Simulated reflection coefficient of single corrugated antipodal Vivaldi antenna.

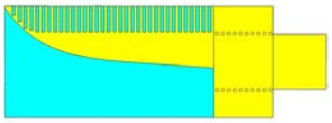

Fig. 7. Simulated corrugated antipodal Vivaldi antenna.

based on [10] while additional tuning is conducted in CST to achieve a low return loss at the 25 GHz operating frequency [11]. The corrugations and antenna features are cut into the metallization layers above and below the dielectric material. Fig. 6 demonstrates the reflection coefficient of a single corrugated antipodal Vivaldi antenna over the frequency range of 23 GHz to 27 GHz in CST. A return loss better than 15 dB can be observed over the full frequency range. Fig. 7 depicts the top metallization layer of a single corrugated antipodal Vivaldi antenna.

The array consists of four antennas spaced at approximately 0.875 λ center to center. In order to attach the antenna array to the Butler matrix, additional SIW feed lines are designed for connection. It can be noted that the 0° phase shifters of the Butler matrix can be modified themselves in order to reduce the overall length of the structure but the implementation of these phase shifters serve to demonstrate that the Butler matrix section can be used as a versatile building block that does not need to be modified for each new array application. An important constraint that must be noted is that the additional feed lines are required to preserve the crucial phase difference that has been produced at the output of the Butler matrix (c.f. Fig. 4). To achieve this, output ports 5 and 8 of the Butler matrix are connected to their respective antennas unimpeded while ports 6 and 7 are tuned with a 0° fixed phase shifter (with reference to the fixed feed lines added to ports 5 and 8). Fig. 8 depicts the full beam-forming network where each of the main components are highlighted. Fig. 9 depicts the manufactured prototype.

In regards to the steering capabilities of this structure, the equation for beam pointing angles is found by (3) and detailed in [3,12]. Let α be the phase difference at the output feedlines, κ is the wave number, and d is the distance between array elements. Calculations for the pointing angles place the main beam lobes at the following four angles: ± 8.2º and ± 25.4º.

$$\beta = \arccos\left(-\frac{\alpha}{\kappa d}\right) - 90^{\circ} \tag{3}$$

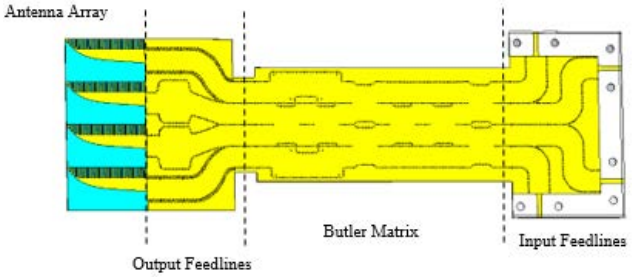

Fig. 8. Simulated beam-forming network.

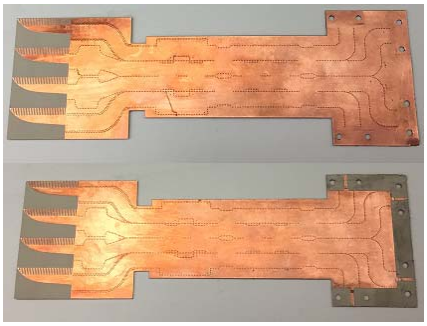

Fig. 9. Top and bottom metallization of beam-forming network.

IV. Results

The beam-forming network is tested in an anechoic chamber using an Anritsu network analyzer. Each input port is excited independently while the remaining ports are terminated with microwave absorbent material. The simulated and measured *S*-parameters of ports 1 and 2 are presented in Fig. 10 through Fig. 12. In Fig. 10, it can be observed that the simulated and measured S_{11} at port 1 is under -10 dB for the full frequency range. The simulated S_{22} peaks above -10 dB around 23.1 GHz and then remains under -10dB for the rest of the spectrum. The measured S_{22} remains below -10 dB for the entire spectrum.

Fig. 11 demonstrates the simulated and measured values of isolation when port 1 is excited. It can be observed that the simulated isolation is better than 10 dB except for the point peaking around 26.4 GHz but is better than 10 dB for the full spectrum when measured. Fig. 12 demonstrates the simulated

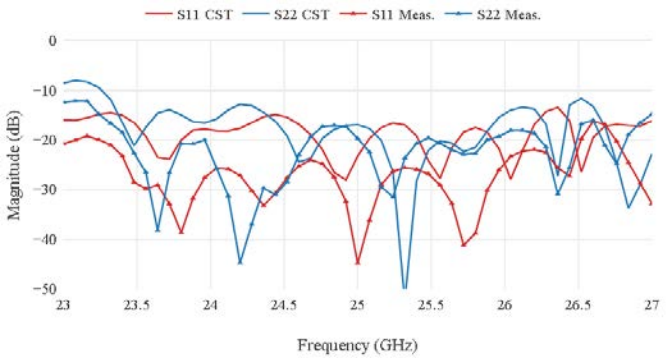

Fig. 10 Simulated and measured reflection coefficients of ports 1 and 2.

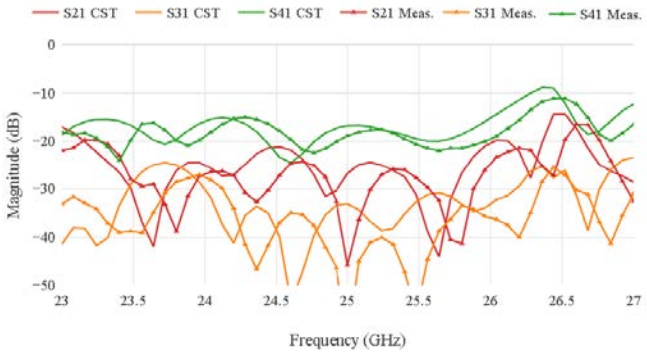

Fig. 11. Simulated and measured results when port 1 is excited.

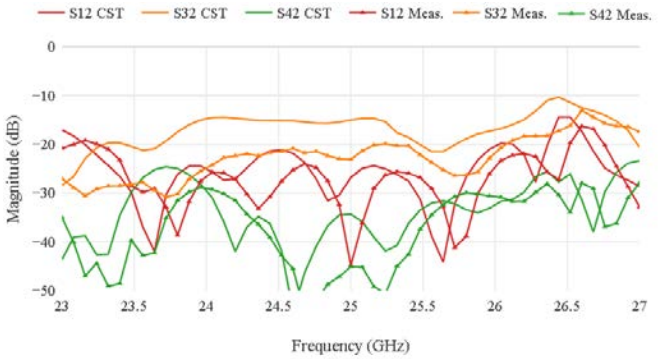

Fig. 12. Simulated and measured results when port 2 is excited.

and measured values of the isolation when port 2 is excited. It can be observed that both the simulated and measured values are better than 10 dB for the full spectrum.

The normalized simulated and measured values of the radiation patterns at 25 GHz are presented in Fig. 13. The measured patterns of each of the main beams form a close resemblance to its simulated beam pattern counterpart. This likeness can be seen particularly below ±45º, but begins to deviate with the port 1 and port 4 side lobes. The measured side lobe levels of ports 1 and 4 rise to a normalized value of -2.4 dB. It can be noted that while this side lobe level is quite high, it is a classic effect caused by a wide (≈ 0.875 λ) spacing between the array elements. The trade off for the high side lobe feature is the ability to suppress the vertical beam component of the end-fire structure. While testing the suppression of the vertical polarization, it was noted that the axis-to-axis cross-polarized electric field component was reduced by approximately 15dB.

Additionally, the gain of the antenna is calculated over the frequency range at the following specified points: 23.5 GHz, 24 GHz, 25 GHz, 26 GHz and 26.5 GHz for both ports 1 and 2. Fig. 14 illustrates a gain of 6.4 dB to 9.2 dB for port 1 and 10 dB to 11.7 dB for port 2. While these results offer differences from the simulations, it can be noted that the measured side lobes in Fig. 13 are slightly wider and differ at high angles by several dB from their simulated values. This relocation of power – along with typical sources of error such as connectors

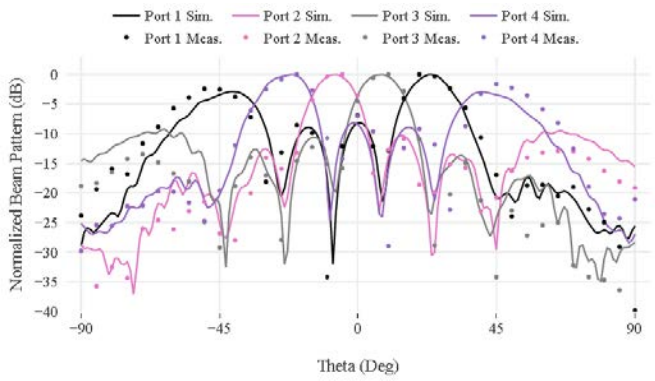

Fig. 13. Simulated and measured normalized beam patterns at 25 GHz.

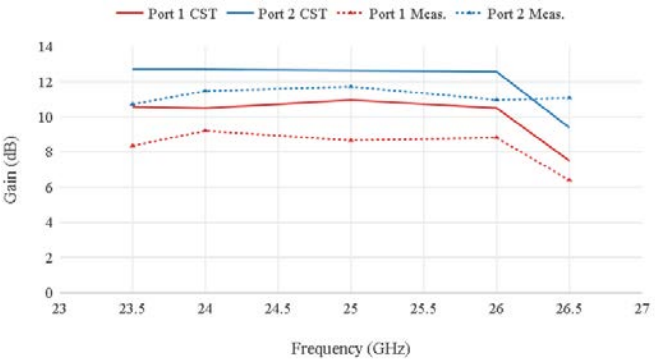

Fig. 14. Simulated and measured gain of ports 1 and 2.

and equipment – can explain the differences observed between simulated and measured gain results.

CONCLUSION

A planar end-fire beam-forming network utilizing corrugated Vivaldi antennas in substrate integrated waveguide technology is presented. The simulated and measured characteristics exhibit good performance in the 25 GHz frequency range. The measured gain over the frequency band for port 1 is in the range of 6.4 dB to 9.2 dB, while the measured gain of port 2 is in the range of 10 dB to 11.7 dB. The results also show good matching between the simulated and measured values for the main beams sweeping a horizon of ±25º.

REFERENCES

[1] D. Deslandes and K. Wu, "Accurate modeling, wave mechanisms, and design considerations of a substrate integrated waveguide*," IEEE Trans. Microw. Theory Tech.*, vol. 54, no. 6, pp. 2516-2526, June 2006.

[2] T. Djerafi, N. J. G. Fonseca, and K. Wu, "Design and implementation of a planar 4 × 4 Butler matrix in SIW technology for wideband applications," in *Proc. Eur. Microw. Conf.*, Paris, France, 2010, pp. 910–913.

[3] Q.-L. Yang, Y.-L. Ban, K. Kang, C.-Y.-D. Sim, and G. Wu, "SIW multibeam array for 5G mobile devices," *IEEE Access,* vol. 4, pp. 2788-2796, 2016.

[4] Q.-L. Yang, Y.-L. Ban, J.-W. Lian, S.-F. Yu, and B. Wu, "SIW Butler matrix with modified hybrid coupler for slot antenna array," *IEEE Access,* vol. 4, pp. 9561-9569, 2016.

[5] N. Tiwari and T. R. Rao, "A switched beam antenna array with Butler matrix network using substrate integrated waveguide technology for 60 GHz wireless communications," *Int. J. Electron. Commun. (AEÜ),* vol. 70, pp. 850-856, 2016.

[6] Y. J. Cheng, P. Chen, W. Hong, T. Djerafi, and K. Wu , "Substrate-integrated-waveguide beamforming networks and multibeam antenna arrays for low-cost satellite and mobile systems," *IEEE Antennas Propagat. Mag.,* vol. 53, no. 6, pp. 18-30, Dec. 2011.

[7] T. Djerafi and K. Wu, "A low-cost wideband 77-GHz planar Butler matrix in SIW technology," *IEEE Trans. Antennas Propagat.,* vol. 60, no. 10, pp. 4949-4954, Oct. 2012.

[8] J. Butler and R. Lowe "Beam-forming matrix simplifies design of electronically scanned antennas," *Electron. Design*, vol. 9, no. 8, pp. 170-173, 1961

[9] Z. Kordiboroujeni and J. Bornemann, "Designing the width of substrate integrated waveguide structures," *IEEE Microw. Wireless Comp. Lett.,* vol. 23, no. 10, pp. 518-520, Oct. 2013.

[10] L. Locke, J. Bornemann, and S. Claude, "Substrate integrated waveguide-fed tapered slot antenna with smooth performance characteristics over an ultra-wide bandwidth," *ACES J.*, vol. 28, pp. 454–462, May 2013.

[11] S. Salem Hesari and J. Bornemann, "Wideband circularly polarized substrate integrated waveguide endfire antenna system with high gain," *IEEE Antennas Wireless Propag. Lett.*, vol. 16, pp. 2262-2265, 2017.

[12] C. A. Balanis, Antenna Theory: Analysis and Design. New York: Wiley Interscience, 2005.